Cite this article as: Kitazawa K., et al. (2023). Cellular Senescence Exacerbates Features of Aging in the Eyes, *AgingBio*, *1*, 1–14. doi: 10.59368/agingbio.20230014.

Research Paper

Cellular Senescence Exacerbates Features of Aging in the Eyes

Koji Kitazawa,[1,2,*] Kohsaku Numa,[1,2] Sandip Kumar Patel,[1] Christina D. King,[1] Akifumi Matsumoto,[2] Chie Sotozono,[2] Pierre-Yves Desprez,[1] Birgit Schilling,[1] and Judith Campisi[1,*]

[1]Buck Institute for Research on Aging, Novato, CA, USA

[2]Department of Ophthalmology, Kyoto Prefectural University of Medicine, Kyoto, Japan

[*]Corresponding authors: kkitazaw@koto.kpu-m.ac.jp; jcampisi@buckinstitute.org

https://doi.org/10.59368/agingbio.20230014

Aging is a process often associated with various age-related diseases. Senescence is one of the hallmarks of aging, and senescent cells acquire a complex, often pro-inflammatory, secretory phenotype termed the senescence-associated secretory phenotype (SASP). Here, we show that ocular surface cells from human cornea become senescent upon X-irradiation, characterized by increased senescence-associated β-galactosidase activity, decreased cell proliferation, increased expression of p16, and disruption of epithelial barrier. Comprehensive transcriptomic and proteomic analysis revealed that human senescent ocular cells (SOCs) acquire an SASP that disrupts epithelial barrier function. During aging in mice, SOCs accumulate, resulting in decreased epithelial barrier and chronic inflammation. Lacrimal gland excision, which leads to symptoms of dry eye (DE), resulted in corneal opacity associated with severe angiogenesis only in aged mice but not in young mice, and early senolytic treatment protected old DE mice from corneal opacity. In conclusion, senescent cells alter the ocular microenvironment through their SASP and eliminating these cells could represent a potential approach to alleviate symptoms associated with aged ocular surface.

Introduction

The aging population is rapidly increasing throughout the world. Aging is a universal process that affects numerous pathological conditions for age-related eye diseases, such as dry eye (DE), cataract, glaucoma, and macular degeneration. We previously investigated the ocular surface changes during aging in humans and mice[1], and observed some senescence-like chronic inflammation, including accumulation of 8-OHdG and lipofuscin-like inclusions, increased expression of p53 and apoptosis-related genes, and decreased Ki67-positive cells[2–6]. However, it was not clear how this chronic inflammation could influence the aged ocular surface, and the causes of this inflammation had yet to be determined.

Hallmarks of aging include genomic instability, telomere attrition, epigenetic alterations, loss of proteostasis, dysregulated nutrient sensing, mitochondrial dysfunction, cellular senescence, stem cell exhaustion, and altered intercellular communication[7]. These age-related changes drive nonpathogenic and chronic low-grade inflammation, which is primarily caused by senescent and immune cells[8]. Cellular senescence is one of the hallmarks of aging and is a cell fate in which both intrinsic and extrinsic signals cause an irreversible cell cycle arrest[9,10], accompanied by many phenotypic changes such as enlarged cell morphology, chromatin reorganization, altered gene expression, and increased glycolytic metabolism and production of reactive oxygen species[11]. Furthermore, senescent cells acquire a complex, often pro-inflammatory, secretory phenotype termed the senescence-associated secretory phenotype (SASP). Among the molecules often secreted by senescent cells are pro-inflammatory cytokines (e.g., IL-6, IL-8, and IL-1b), chemokines (e.g., CXCL5 and CXCL10), and matrix metalloproteinases (MMPs) (e.g., MMP1, MMP3, and MMP9)[12,13]. These molecules are frequently associated with a variety of age-associated pathologies, including many that are characterized by chronic inflammation[14–16]. Ocular surface inflammation promotes conjunctival squamous metaplasia[17] and inflammation-associated barrier dysfunction[18], resulting in the development of refractory corneal diseases. However, the causes of inflammation at the ocular surface and how the ocular surface is altered during aging are still to be determined.

In this study, we established cell culture and mouse models to examine the phenotype of human senescent ocular cells (SOCs) and the role of senescent cells in aged ocular surface *in vivo*. We show that accumulation of cellular senescence at the ocular surface is associated with chronic inflammation and disruption of the epithelial barrier, leading to refractory ocular surface diseases, including corneal opacity, associated with severe angiogenesis.

Materials and Methods

Cell cultures and treatments

We used primary corneal epithelial cells (CoC) isolated from human donor corneas (CorneaGen, Seattle Eye Bank, WA). CoC were isolated and cultured as previously described[19], with minor modifications. Corneas and conjunctivas were treated with Dispase type II (Godo Shusei, Tokyo, Japan) at a concentration of 1000 PU/ml at 4°C overnight, and corneal/conjunctival

epithelium was peeled off. CoC were then dissociated using TrypLE™ Express (Thermo Fisher Scientific, Waltham, MA) for 5 min at 37°C and seeded onto each well of six-well plates. CoC were cultured at 37°C at 95% humidity and 5% CO_2 in complete CoC medium[20], consisting of Dulbecco's modified Eagle's and Ham's F-12 media (DMEM/F12, 1:1 mixture) (Thermo Fisher Scientific), B-27™ supplement (2%) (Thermo Fisher Scientific), Rho-kinase inhibitor Y-27632 (10 μM) (Selleck Chemicals, Houston, TX), keratinocyte growth factor (10 ng/ml) (Thermo Fisher Scientific), and penicillin-streptomycin (50 IU/ml) (Nacalai Tesque). Cultured CoC were used for subsequent experiments after one passage using TrypLE™ Express (Thermo Fisher Scientific) at room temperature (RT) upon reaching sub-confluence.

We generated SOC from primary human corneal and conjunctival cells using ionizing radiation (IR) (10 Gy) or the chemotherapeutic agent DOXO (250 nM for 24 h), which intercalates into DNA and disrupts topoisomerase-II-mediated DNA repair[21,22]. SOCs were cultured for 10 days to allow the development of a full senescent phenotype. Mock-treated cells or cells treated with Dimethylsulfoxide were used as controls.

SA-β-gal staining and EdU labeling

Cells were fixed and processed for SA-β-gal staining as per the manufacturer's instruction (Biovision, Waltham, MA). A Nikon Eclipse E800 microscope was used for imaging, and images were quantified using Image J software. Cell proliferation was evaluated by incorporation of EdU and the Click-iT EdU Cell Proliferation Assay Kit (Invitrogen). Briefly, cells were given 10 μM EdU for 24 hours before fixation, permeabilized and incubated with Click-iT reaction cocktail as per the manufacturer's instruction. A microscope (Nikon Eclipse E800) was used for imaging, and images were quantified using Image J software. More than 100 cells from 5 different fields were quantified per condition, and all experiments were done in triplicate.

Quantitative reverse transcription polymerase chain reaction (qRT-PCR) analysis

RNA was isolated from cultured cells and homogenized tissues using the Bioline Isolate II RNAMini Kit (Meridian Bioscience, Cincinnati, OH) as recommended by the supplier. Complementary DNA was synthesized from 500 to 1000 ng of total RNA using High-Capacity cDNA Reverse Transcription Kit (Thermo Fisher Scientific). qRT-PCR was performed using the LightCycler® 480 Real-Time PCR System (Roche Applied Science, Penzberg, Germany), as described previously[23]. The $2\times-\Delta\Delta Ct$ method was used to calculate expression levels normalized to human or mouse beta actin (ACTB) Endogenous Control (Thermo Fisher Scientific). All the primers used for the experiments are listed in **Tables S6 and S7**.

Conditioned media

Irradiated CoC or non-senescent (NS) mock cells were cultured in complete media, washed three times with phosphate-buffered saline (PBS), and placed in DMEM/F12 (serum- and supplement-free media) (Thermo Fisher Scientific) for two days. Subsequently, cells were washed with PBS and placed in phenol red-free DMEM/F12, and conditioned medium (CM) was collected after 24 hours. A total of 150,000 cell equivalents/ml of CM were used for barrier function assays. Collected CM was also used for mass spectrometry (MS) analysis.

Cell viability assay upon ABT263 treatment

To determine the dose of ABT263 (Selleck Chemicals, Houston, TX) that specifically kills SOCs and not NS cells, cell viability was assessed using the cell counting kit-8 (Dojindo Molecular Technologies, Inc., Rockville, MD). SOC or NS cells were incubated in complete media plus 10% cell viability kit reagent, 150 μl/well in 96-well plates, for 2 hours at 37°C. Supernatants were transferred to new 96-well plates and absorbance read at 450 nm. For the subsequent culture experiments, fresh complete media containing or not ABT263 were used.

Immunofluorescence staining

Fresh tissues from normal mouse corneas were embedded in Tissue-Tek OCT, cryopreserved, and sectioned (7 μm). Immunostaining of corneal sections was performed according to a previously reported method[24] with modifications. Briefly, cryosections were incubated at RT for 1 min and then fixed with 4% paraformaldehyde at 4°C for 10 min. After aspiration of the fixative, sections were rinsed with PBS for 5 min and permeabilized with 0.05% Triton-X-100 at RT for 30 min. Samples were blocked with 10% goat serum at RT for 45 min and then incubated with F4/80 primary antibody (Abcam, #ab6640, 1:200 dilution) overnight at 4°C. The next day, samples were washed with PBS and incubated with a secondary antibody (Invitrogen, Alexa Fluor 594-conjugated anti-rat IgG) at a dilution of 1:1000 for 1 hour at RT. After washing, 4′, 6-diamidino-2-phenylindole was added. Sections were viewed using a fluorescence microscope (Nikon Eclipse E800) and photographed.

Western blotting

Cells were washed with ice-cold PBS and lyzed with Radio-Immunoprecipitation Assay buffer supplemented with 2-mercaptoethanol (final concentration 6%) and Halt Protease and Phosphatase Inhibitor Cocktail (Thermo Fisher Scientific), then boiled for 5 min at 95°C. Equal amounts (10–30 μg) of samples were loaded, and proteins were separated by sodium dodecyl-sulfate polyacrylamide gel electrophoresis using 4%–12% Bis-Tris gels (Bio-Rad, Hercules, CA), followed by transfer to polyvinylidene fluoride membranes using iBlot Dry Blotting Gel Transfer System (Thermo Fisher Scientific). Membranes were blocked for 1 hour in 5% bovine serum albumen-Tris-buffered saline with 0.1% Tween® 20 detergent (TBST) or 5% milk-TBST at RT and then incubated with primary antibodies overnight at 4°C. Blots were washed and incubated with horseradish peroxidase (HRP)-conjugated secondary antibodies for 1 hour at RT, and detection was performed using enhanced chemiluminescence. Primary antibodies were against p16 (Abcam, #ab108349, 1:500 dilution) and HMGB1 (Abcam, #ab18256, 1:500 dilution). Secondary antibodies were HRP-conjugated goat anti-rabbit (Bio-Rad) and goat anti-mouse (Bio-Rad) antibodies. An antibody against beta actin (Sigma, #A2228, 1:10,000 dilution) was used for loading control.

Barrier function in culture

To measure barrier function of ocular surface cells, we used a volt-ohm meter (EVOM, World Precision Instruments), as we previously reported[25]. NS CoC or SOCs cultured with NS at a ratio of 75%–25% were seeded at a cell density of 100,000 cells per well in 24-well transwell plates (Corning, 24-mm Transwell with 0.4-μm Pore Polyester Membrane Insert). Upon reaching 100% confluence, cells were tested for transepithelial electrical resistance (TEER) between the upper and lower chambers of

permeable cell culture inserts using the volt-ohm meter. The TEER was measured and calculated by multiplying the measured resistance (ohms) by the growth area of the transwell filter. The background resistance due to the filter alone was subtracted from each of the measurements. The TEER was measured twice, and the average value was used for analysis.

Next-generation RNA-seq

An initial quality assessment of raw RNA-seq data was performed using FastQC (v0.12.1)[26] to evaluate read quality. TrimGalore (v4.3)[27] was conducted to remove adapter sequences and low-quality reads. The trimmed reads were aligned to the reference genome (GRCh38) using HISAT2 (v2.2.1)[28]. We converted the output SAM files to sorted BAM files with SAMtools (v1.12)[29] for downstream analysis. FeatureCounts (v2.0.3)[30] was utilized to assign mapped reads to their corresponding genes, generating count data for each gene. The raw read counts were normalized using DESeq2 (v1.8.3)[31]. We performed differential gene expression analysis with DESeq2 (v1.8.3) in R (v4.2.3) and RStudio (v2023.03.0+386). Gene ontology (GO) and pathway analysis for the identified differentially expressed genes (DEGs) were carried out using the clusterProfiler (v4.6.2) package.

Isolation of corneal SASP proteins

A detailed list of reagents and resources used in the proteomics analysis, including vendors and catalog numbers, is available in the Reagent and Resource Table (**Table S8**). Briefly, protein sample processing was performed as follows. Conditioned media from corneal cells (quiescent control and IR-treated cells [n = 3 each]) were collected as previously described[13]. Salt and other media components were removed using 3 kDa cutoff columns (Amicon Centrifugal Filters), and SASP protein extracts were subsequently lyzed using lysis buffer (5% SDS and 50 mM TEAB). Each extract was reduced by incubation with 20 mM dithiothreitol in 50 mM TEAB for 10 min at 50°C, and subsequently alkylated with 40 mM iodoacetamide in 50 mM TEAB for 30 min at RT in the dark. Extracts were acidified to yield pH < 1 using phosphoric acid (v/v), and subsequently, 100 mM TEAB in 90% methanol were added.

The entire protein extracts were spun through the micro S-Trap columns (Protifi). Subsequently, the S-Trap columns were washed with 90% methanol in 100 mM TEAB, placed in clean elution tubes and incubated with trypsin digestion buffer (50 mM TEAB, pH ~8) at a 1:25 ratio (protease:protein, wt:wt) overnight. Peptides were then sequentially eluted with 50 mM TEAB and 0.5% formic acid (FA), and 50% acetonitrile (ACN) in 0.5% FA. Both fractions were pooled together, vacuum dried, and resuspended in 0.2% FA for desalting. The desalted peptides were concentrated and resuspended in aqueous 0.2% FA for MS-based quantitative analysis.

Mass spectrometric data-independent acquisition (DIA)

Eight microliters of each sample were diluted with 2% ACN in 0.1% FA to obtain a concentration of 400 ng/μL. One microliter of indexed Retention Time Standard (iRT, Biognosys, Schlieren, Switzerland) was added to each sample as internal standard, thus bringing up the total volume to 20 μl[32]. Reverse-phase high-pressure liquid chromatography (HPLC)-MS/MS analyses were performed on a Dionex UltiMate 3000 system coupled online to an Orbitrap Exploris 480 mass spectrometer (Thermo Fisher Scientific, Bremen, Germany). The solvent system consisted of 2% ACN, 0.1% FA in water (solvent A) and 80% ACN, 0.1% FA in ACN (solvent B).

Digested peptides (400 ng) were loaded onto an Acclaim PepMap 100 C_{18} trap column (0.1 × 20 mm, 5 μm particle size; Thermo Fisher Scientific) over 5 min at 5 μl/min with 100% solvent A. Peptides (400 ng) were eluted on an Acclaim PepMap 100 C_{18} analytical column (75 μm × 50 cm, 3 μm particle size; Thermo Fisher Scientific) at 300 nl/min using the following gradient: linear from 2.5% to 24.5% of solvent B in 125 min, linear from 24.5% to 39.2% of solvent B in 40 min, up to 98% of solvent B in 1 min, and back to 2.5% of solvent B in 1 min. The column was re-equilibrated for 30 min with 2.5% of solvent B, and the total gradient length was 210 min. Each sample was acquired in DIA mode[33–35]. Survey MS1 spectra were collected at 120,000 resolution (automatic gain control [AGC] target: 3e6 ions, maximum injection time: 60 ms, 350–1,650 m/z), and MS2 spectra at 30,000 resolutions (AGC target: 3e6 ions, maximum injection time: Auto, Normalized Collision Energy: 30, fixed first mass 200 m/z). The isolation scheme consisted of 26 variable windows covering the 350–1,650 m/z range with a window overlap of 1 m/z[34].

DIA data processing and statistical analysis

DIA data were processed in Spectronaut v15 (version 15.1.210713.50606; Biognosys) using directDIA. Data were searched against the *homo sapiens* proteome with 42,789 protein entries (UniProtKB-TrEMBL), accessed on 12 July 2021. Trypsin/P was set as digestion enzyme, and two missed cleavages were allowed. Cysteine carbamidomethylation was set as fixed modification, and methionine oxidation and protein N-terminus acetylation as variable modifications. Data extraction parameters were set as dynamic. Identification was performed using 1% precursor and protein q-value (experiment). Quantification was based on MS2 area, local normalization was applied, and iRT profiling was selected. Differential protein expression analysis was performed using a paired t-test, and q-values were corrected for multiple testing, specifically applying groupwise testing corrections using the Storey method[36]. Protein groups with at least two unique peptides, q-value < 0.05, and absolute Log2 (fold-change) > 0.58 were considered to be significantly altered and are listed in **Table S2**.

Animals

Animal studies were conducted in compliance with protocols approved by the Institutional Animal Care and Use Committee of the Buck Institute for Research on Aging. Animals were maintained in a controlled environment (20°–22°C; 12-hour light:12-hour dark cycle). We engineered a bacterial artificial chromosome in which the p16 promoter drives the expression of a fusion protein (3MR) containing Renilla luciferase, red fluorescent protein (RFP), and a herpes simplex virus thymidine kinase (HSV-TK). RFP enables the sorting of 3MR-expressing cells from tissues. HSV-TK enables the elimination of 3MR-expressing cells using ganciclovir (GCV), a nucleoside analog that has a high affinity for HSV-TK, but low affinity for cellular TK, and is converted into a toxic moiety by the HSV-TK[37–39]. C57BL/6 mice or p16-3MR mice were used in this study. To eliminate senescent cells in p16-3MR homozygous female mice, 0.3% topical GCV treatment was performed, whereas topical PBS treatment was used as control.

Lacrimal gland excision (LGE)

Animals were placed under general anesthesia using 3% isoflurane. Incisions anterior to the ear were performed to expose the external lacrimal gland. Lacrimal glands were excised from the orbit using ophthalmic forceps with the aid of a stereoscopic microscope. Gland excisions were performed on both right and left sides. After surgery, mice were evaluated for corneal surface integrity after application of fluorescein, and tear production was assessed as described below.

Tear volume and corneal fluorescein staining *in vivo*

The tear storage volume of each eye was measured twice with phenol-red impregnated cotton threads (Zone-Quick; FCI Ophthalmics) and was averaged as an index of the tear retaining action. The cotton thread was placed on the ear conjunctiva of the mouse, and the amount of the tears was measured for 15 sec, followed by immediately measuring the length of the wet portion of the thread. To evaluate the barrier function of the corneal epithelium, corneal epithelial damage was assessed with fluorescein staining under the handy slit lamp with blue filter illumination (XL-1; Reexam). A corneal fluorescein staining score was assigned at each 1/3 area of the cornea (upper, intermediate, and lower). The score was categorized from 0 to 3 (0 = no fluorescence, 1 = fluorescence evident as sparse dots, 2 = dense dot-like fluorescence pattern, and 3 = very dense dot-like fluorescence) assessed by an unbiased observer, as previously reported[40].

Statistics

All data with error bars are presented as mean ± Standard error of the mean, and the individual data points (dots) are presented in the bar graphs. Statistical analyses were performed using Prism 9 software with 9.2.0 (283) (GraphPad, La Jolla, CA, USA). Comparisons between groups were conducted with one-way analysis of variance, followed by the post hoc Dunnett's multiple comparison test. Welch's adjusted t-test (also called unequal variances t-test), a modified Student's t-test, was also used under the assumption of unequal variances. Most of cell culture experiments were done in triplicate and reproduced at least three times independently.

Results

Role of human SOCs in the inflammatory phenotype at the ocular surface

The ocular surface is composed of cornea, conjunctiva, and tear fluid. Accumulation of senescent cells during aging is part of the hallmarks of aging. In order to characterize the features of SOC, we induced cellular senescence in human primary CoC upon treatment with a DNA-damaging agent, IR. Irradiated human SOCs showed higher senescence-associated β-galactosidase staining and lower incorporation of EdU than nonirradiated cells, indicating cellular senescence induction (Fig. 1a). Irradiated human SOCs secreted pro-inflammatory factors that are part of the SASP, which are also expressed by several types of senescent cells. These factors included *IL-6*, *IL-1β*, *MMP-3*, *MMP-9*, and *TNF-α*, in addition to the expected upregulation of the cell cycle inhibitors $p16^{INK4a}$ (p16) and $p21^{WAF1/Cip1}$ (p21), and downregulation of the nuclear protein *LMNB1* and HMGB1, at mRNA levels (Fig. 1b,d) and protein levels (Fig. 1c), as we previously reported in other cell types undergoing senescence[12,41–43]. These data show that human ocular cells undergoing DNA damage acquire an SASP, which could potentially be causal to the inflammation detected at ocular surfaces during aging.

Disruption of the corneal epithelial barrier by SOC

The ocular surface evolved to protect the cornea and keep it smooth and wet, a prerequisite for proper eyesight. With age, the ocular surface becomes more vulnerable to external stimuli[44], as is the case for many other tissues. In order to examine the effects of SOC on epithelial barrier function, the TEER was measured. SOC were cocultured with control NS at a ratio of 75 to 25, with cells being fully confluent in culture inserts. SOC appeared larger than NS (Fig. 2a), and TEER readings in cocultures were lower compared to NS cultures (Fig. 2b). Next, we determined whether the decrease in TEER was due to SOC themselves or to the SASP they secrete. CM from SOC, which contained the SASP, was collected and added to NS to determine whether the TEER would be modified. CM collected 3 days after senescence induction triggered a significant decrease in TEER readings (Fig. 2c), suggesting that some SASP factors disrupt the corneal epithelial barrier, which is a key component of ocular surface.

To confirm that senescent cells are responsible for the disruption of barrier function, we tested whether the decrease in TEER was reversed upon removal of senescent cells with a senolytic drug, ABT263. ABT263 is a B-cell lymphoma 2 inhibitor and started to kill SOC selectively three days after the initiation of treatment. Cell viability of SOC was decreased by 70% compared to NS at 0.1 μM of ABT263 on day 7 of the treatment (Fig. 2d). The improvement in TEER was consistent with the effect of ABT263 on SOC overtime, and on day 7, the values reached levels close to control NS (Fig. 2e). Overall, our data suggest that SOC contribute to the disruption of the corneal epithelial barrier through the secretion of SASP factors. We determined that not only inflammatory cytokines but also chemokine-related genes, such as *CCL2*, *CXCL3*, *CXCL8*, *CXCL9*, and *CXCL10*, were highly expressed by SOC compared to NS (Fig. 2f).

Next, we analyzed the global gene expression profile of SOC using RNA-seq as an unbiased approach. Global differential expression analyses between SOC and NS revealed 3,234 DEGs significantly, with $|\log FC| > 1.0$ and an adjusted p-value < 0.05 (Fig. 2g, **Table S1**). A comparison of SOC and NS showed that a high proportion of the DEGs, that is, 2,102 genes, were upregulated and 1,132 genes were downregulated in SOC. Downregulated genes are significantly associated with enriched GO terms related to organelle fission, nuclear division, DNA replication, and mitotic cell cycle phase transition (Fig. 2h, **Table S2a**), which are all modulated during cellular senescence. Upregulated genes are significantly associated with enriched GO terms related to positive regulation of leukocyte migration and chemotaxis, and extracellular structure organization (Fig. 2i, **Table S2b**), suggesting that SOC acquires an inflammatory phenotype. Moreover, MMP genes, such as *MMP8*, *MMP12*, *MMP7*, *MMP24*, *MMP15*, *MMP10, MMP3*, and *MMP1*, were upregulated, which could explain the disruption of the corneal epithelial barrier (Fig. 2b,c).

Characterization of the SASP components secreted by SOC

The SASP exhibits multifunctional aspects and depends on the cell types[13], physiological states[41], and environmental stimuli[45]. We therefore analyzed the SASP factors secreted by SOC using a label-free, unbiased quantitative mass spectrometric approach, referred to as DIA[35]. The proteomics analysis of conditioned

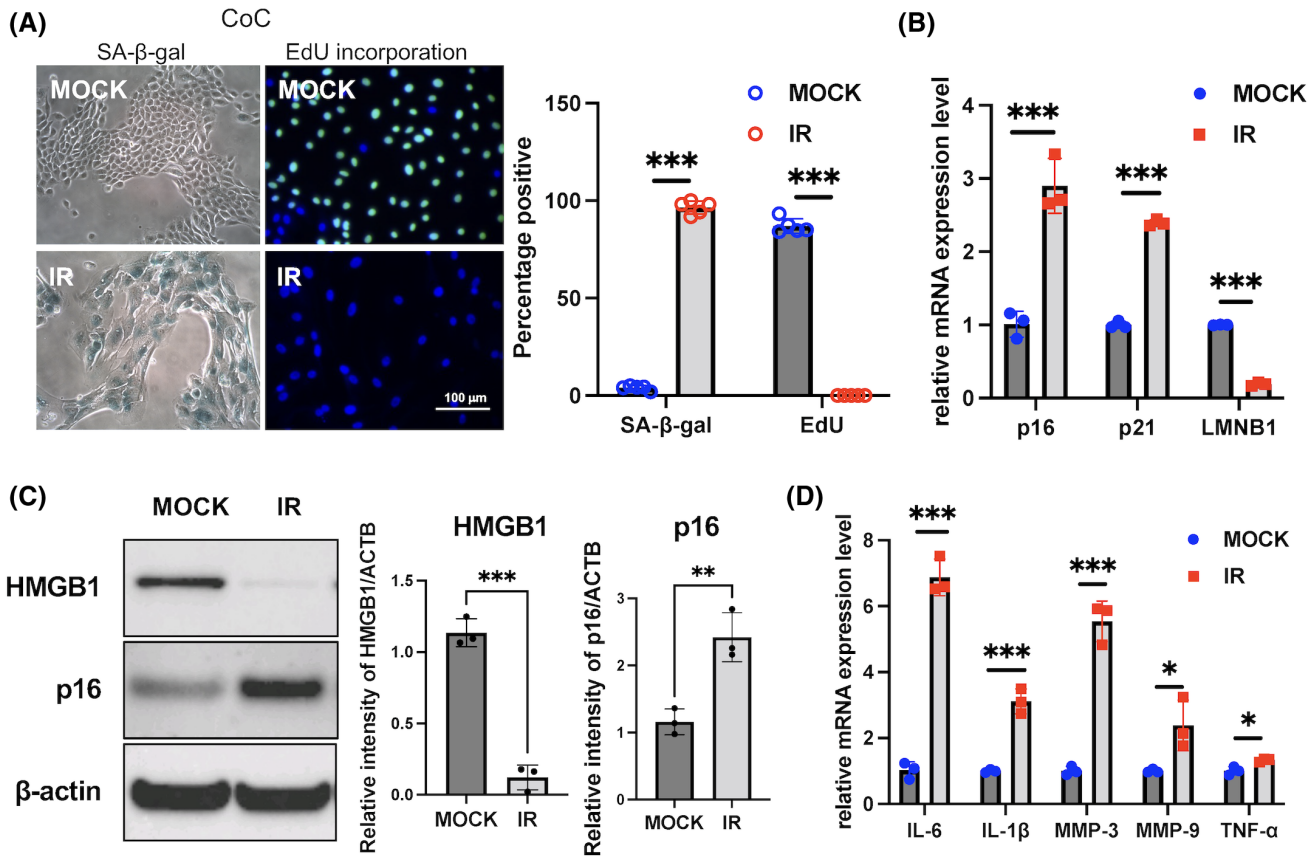

Figure 1. Characteristics of human senescent ocular cell (SOC). (A) senescence-associated β-galactosidase (SA-β-Gal) staining and EdU labeling of corneal epithelial cells (CoC) upon ionizing radiation (IR)-induced senescence. CoC were treated with 10 Gy IR (or mock as control) and cultured for 10 days. SA-β-Gal expression and EdU labeling were performed 10 days after treatment. Representative images are shown (left) and results are plotted as mean % of positive cells from five independent experiments (right). **(B)** Using real-time polymerase chain reaction (PCR), RNA expression analysis of *p16*, *p21*, and *LMNB1* in control cells, and IR-treated cells from human cornea. **(C)** Protein expression analysis and quantification of p16 and HMGB1 in control cells and IR-treated cells from human cornea using western blotting. **(D)** Using real-time PCR, RNA expression analysis of senescence-associated secretory phenotype (SASP) factors (*IL-6*, *IL-1β*, *MMP-3*, *MMP-9*, *TNF-α*) in control cells and IR-treated cells from cornea. Results were plotted as mean and standard deviation from three independent experiments. Gene expression was normalized to the housekeeping gene *Actb*. * = $p < 0.05$; ** = $p < 0.01$; *** = $p < 0.001$.

media from human SOC and mock revealed 636 quantifiable proteins (≥2 unique peptides) (**Table S3a**). Partial least squares-discriminant analysis clustered IR-induced senescence and mock corneal SASP, and 91% variate contributed to this conclusion (**Fig. S1a,b**). Out of 639 quantifiable corneal SASP proteins, 609 proteins were significantly altered in senescence compared to mock (fold change ≥ 1.5, q-value ≤ 0.05) as shown in **Table S3b** and Fig. 3a, of which 429 proteins showed strong secretion, and 180 proteins were decreased as presented in the volcano plots. Furthermore, to emphasize the heterogeneity of the SASP profiles in different cell types, we compared the corneal epithelial SASP with the IR-induced SASP from human lung fibroblasts (IMR90 cells) as shown previously[13]. We determined that 427 and 367 SASP proteins were unique to epithelial cells and fibroblasts, respectively (Fig. 3b), while 179 SASP proteins overlapped (Fig. 3b, **Table S3**). Based on the present analysis, growth differentiation factor 15 (GDF15), MMPs, and SERPIN proteins are integral to SASP from both epithelial cells and fibroblasts (**Table S4**), as we previously reported[13], suggesting that multiple senescent cell types exhibit some important and common SASP factors.

The top 10 corneal SASP proteins showing increased and limited secretions are presented in Fig. 3c and **Table S2b**, and some of the most promising candidate factors for the biological effects of SOC, which include GDF15, calcyphosin (CAPS), lumican (LUM), and latent transforming growth factor beta binding protein 3 (LTBP3), are displayed in Fig. 3d. GDF15 belongs to the transforming growth factor-beta (TGF-β) superfamily proteins, which are highly expressed in human aged corneas[46]. We found that GDF15 was upregulated in SOC both at RNA levels (Fig. 3e, **Table S1b**) and at secreted protein levels (Fig. 3f). CAPS is a calcium/metal-binding protein increased during cellular senescence[47], LUM is a keratan sulfate proteoglycan of the small leucine rich proteoglycan family originally identified in cornea, and LTBP3 is a key regulator of TGF-β1, -β2, and -β3.

Functional analysis using GO term revealed that ubiquitin-dependent degradation of cyclin D1, p53-independent DNA damage response, and G1/S DNA damage checkpoint pathways associated with senescence-induction were upregulated (Fig. 3g, **Fig. S2**, **Table S5a**). Upregulation of the immune system and interleukin signaling suggests a role of the SASP in the inflammation at the ocular surface, possibly via inflammatory cell infiltration within ocular tissue (Fig. 3g, **Fig. S2**). Moreover, upregulation in metalloaminopeptidase activity and keratinization-related proteins (Fig. 3g, **Fig. S2**) and downregulation of axon- and neuron-projection regeneration could be associated with loss of biological

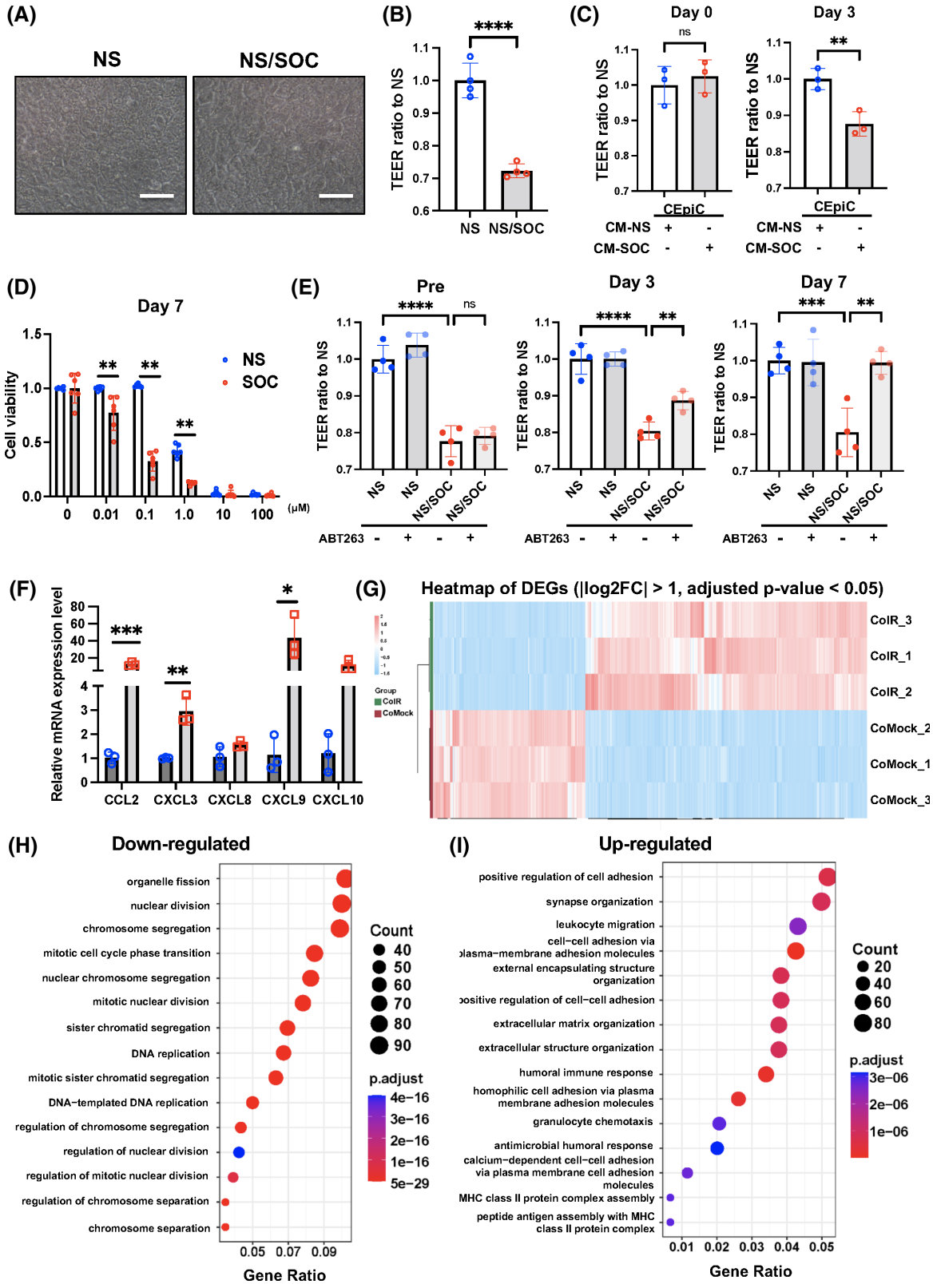

Figure 2. Measurement of transepithelial electrical resistance (TEER) as an epithelial barrier in human CoC and effects of a senolytic agent. **(A)** Senescent human CoC (SOC, IR-treated cells) were seeded together with non-senescent (NS) human CoC (NS, mock-treated cells) at a ratio of 3/1 in the upper wells of transwell plates. **(B)** The TEER of NS alone or SOC together with NS was measured. **(C)** Human CoC were seeded, and, after reaching cell confluency, the conditioned medium (CM) from NS or SOC were added, and the TEER measured until day 3 post CM treatment. **(D)** Timeline of cell viability assay upon ABT263 treatment. Cells were treated with IR or mock, and then treated with ABT263 at 0, 0.01, 0.1, 1.0, 10, and 100 μM. Cell viability was analyzed at day 7. Results were plotted as mean and standard deviation from six independent experiments. The average value at 0 μM for

(legend continued on next page)

each group was set at 100% cell viability. **(E)** SOCs were seeded with NS at a ratio of 3/1 in the upper wells of transwell plates, treated with the senolytic agent ABT263 at 0.1 μM, and their TEER measured overtime. Results were plotted as mean and standard deviation from four independent experiments. **(F)** Using real-time PCR, RNA expression analysis of chemokine-related genes (*CCL2*, *CXCL3*, *CXCL8*, *CXCL9*, and *CXCL10*) in control cells and IR-treated cells from human cornea. **(G)** Heat map of differential gene expressions comparing NS and SOCs. **(H)** Pathway and network analysis of gene expressions that are significantly decreased in SOCs compared to NS. **(I)** Pathway and network analysis of gene expressions that are significantly increased in SOCs compared to NS. Gene expression was normalized to the housekeeping gene *Actb*. * = $p < 0.05$; ** = $p < 0.01$; *** = $p < 0.001$.

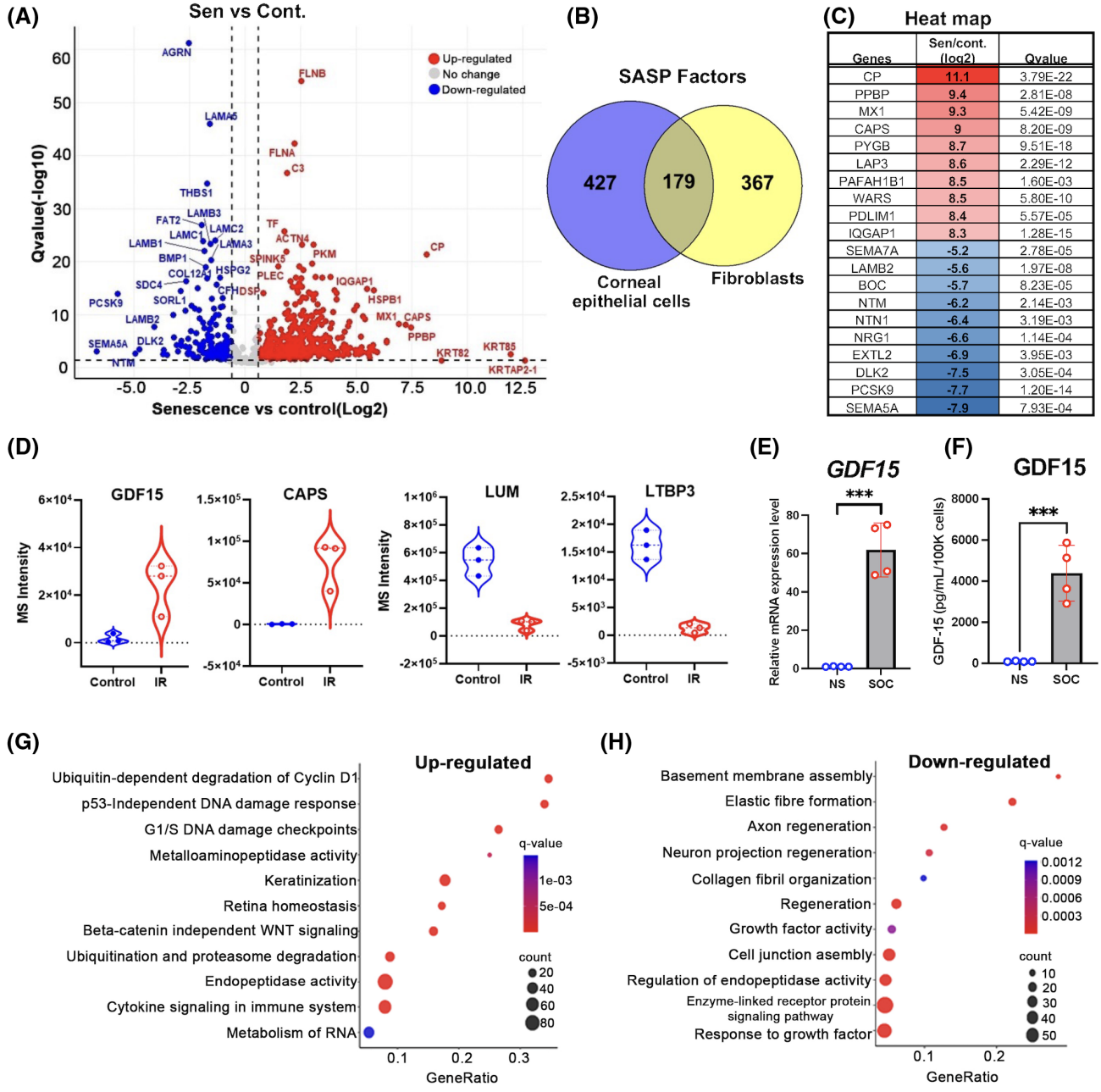

Genes	Sen/cont. (log2)	Qvalue
CP	11.1	3.79E-22
PPBP	9.4	2.81E-08
MX1	9.3	5.42E-09
CAPS	9	8.20E-09
PYGB	8.7	9.51E-18
LAP3	8.6	2.29E-12
PAFAH1B1	8.5	1.60E-03
WARS	8.5	5.80E-10
PDLIM1	8.4	5.57E-05
IQGAP1	8.3	1.28E-15
SEMA7A	-5.2	2.78E-05
LAMB2	-5.6	1.97E-08
BOC	-5.7	8.23E-05
NTM	-6.2	2.14E-03
NTN1	-6.4	3.19E-03
NRG1	-6.6	1.14E-04
EXTL2	-6.9	3.95E-03
DLK2	-7.5	3.05E-04
PCSK9	-7.7	1.20E-14
SEMA5A	-7.9	7.93E-04

Figure 3. Unbiased quantitative proteome profile of human corneal SASP. (A) CM from IR-induced senescent human CoC (SOC) (n = 3) and NS human CoC (control) (n = 3) were fractionated using HPLC and analyzed using mass spectrometry (MS). Volcano plot showing Q values (−log10) versus fold change of (log2) SOC and control CoC. Blue, downregulated; red, upregulated; and black, no significant change (≥2 unique peptides, fold change ≥ 1.5, q-value ≤ 0.05). **(B)** Venn diagram showing unique and integral significantly altered SASP proteins (≥2 unique peptides, fold change ≥ 1.5, q-value ≤ 0.05) in IR-induced CoC and human lung fibroblast cells (IMR-90). **(C)** Table showing top 10 up or downregulated cornea SASP proteins. **(D)** Violin plot showing the individual differential expression of growth differentiation factor 15 (GDF15), calcyphosin (CAPS), lumican (LUM), and latent transforming growth factor beta binding protein 3 (LTBP3) comparing quiescent controls and SOCs. Results are shown as biological replicates and mean ± SD, and paired t-test showed significant differences between groups. **(E)** Using real-time PCR, RNA expression analysis of *GDF15* in SOCs compared to NS. Gene expression was normalized to the housekeeping gene *Actb*. **(F)** ELISA analysis of GDF15 protein expression in corneal SASP. **(G)** Pathway and network analysis of secreted proteins that are significantly increased in corneal SASP. **(H)** Pathway and network analysis of secreted proteins that are significantly decreased in corneal SASP. *** = $p < 0.001$.

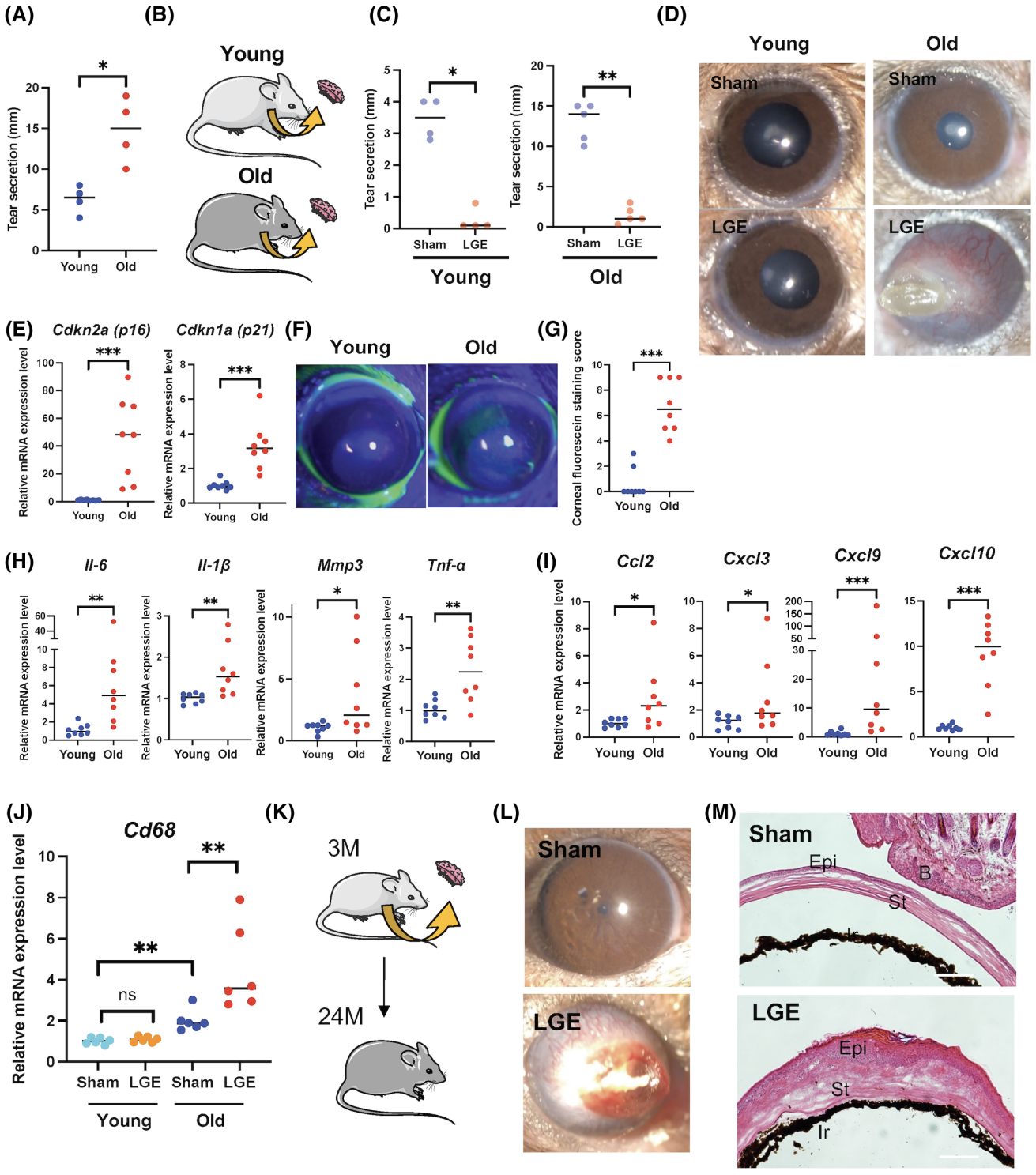

Figure 4. Changes at the ocular surface after lacrimal gland excision (LGE) in young and old mice. **(A)** Tear secretion was measured using the cotton thread with phenol red in eyes of young mice (n = 4) and old mice (n = 4). **(B)** LGE was performed on the right side and sham surgery on the left side of young mice (4 months of age) and old mice (24 months of age). **(C)** Tear secretion was measured using the cotton thread with phenol red in eyes of young mice post sham control (n = 4) or after LGE (n = 4) and old mice post sham control (n = 5) or after LGE (n = 5). **(D)** Representative slit-lamp images of ocular surfaces in young or old control mice and in young or old mice one month after LGE surgery. **(E)** Using real-time PCR, RNA expression analysis of *p16* and *p21* in cornea of young mice (4 months of age) and old mice (24 months of age). **(F)** Representative corneal fluorescein staining images in young and old mice. **(G)** Corneal epithelial damage was assessed with fluorescein staining. A corneal fluorescein staining score was assigned with 1 to 3 at each 1/3 area of the cornea (upper, intermediate, and lower), in young mice (4 months of age) and old mice (24 months of age). **(H)** Using real-time PCR, RNA expression analysis of SASP-related genes including *Il-6*, *Il-1β*, *Mmp3*, and *Tnf-α* in cornea from young and old mice. **(I)** Using real-time PCR, RNA expression analysis of various chemokine-related genes including *Ccl2*, *Cxcl3*, *Cxcl9*, and *Cxcl10* in cornea from young and old mice. **(J)** Using real-time PCR, RNA expression analysis of *Cd68* and *F4/80* in cornea from young and old mice post sham control (n = 6) or after LGE (n = 6). **(K)** Old mice (24 months of

(legend continued on next page)

age) post sham or LGE performed at young age (3 months) were used. **(L)** Representative slit-lamp images of ocular surfaces and corneal fluorescein staining images in old mice (24 months of age) with or without LGE surgery. **(M)** Representative hematoxylin and eosin stain images of ocular surfaces. Ocular features post sham control or after LGE include cornea opacity, angiogenesis and keratinization. Gene expression was normalized to the housekeeping gene *Actb*. * = $p < 0.05$; ** = $p < 0.01$; *** = $p < 0.001$.

function in SOC (**Fig. 3g,h**, **Fig. S3**, **Table S5b**). Interestingly, downregulation of cell junction assembly could lead to the disruption of barrier function in CoC, a function that is vital for a healthy eye (**Fig. 3h**).

Comparison of ocular surfaces using a DE model in young and old mice

We investigated the potential link between the presence of senescent cells and an age-related ocular surface disease (DE). We determined that the tear fluid volume was higher in old mice than in young mice (**Fig. 4a**), unlike humans as previously reported[48,49]. Thus, we created a mouse model of severe DE in young mice (4 months of age) and old mice (24 months of age) (**Fig. 4b**). Extraorbital LGE provides a simple and consistent model of severe aqueous tear-deficient DE. LGE results in tear film instability, which, importantly, plays a central role to all forms of DE[40,50–53]. Tear fluid secretion was measured after LGE, and we determined that tear fluid volume was significantly lower in the LGE-treated eyes compared to sham eyes in both young and old mice (**Fig. 4c**). The anterior segment photographs show that transparency was maintained in young eyes. However, LGE-treated eyes in old mice displayed corneal opacity with severe angiogenesis (**Fig. 4d**). In addition to corneal opacity associated with angiogenesis, 60% of LGE-treated eyes displayed corneal keratinization (**Fig. 4d**).

We found that SOC in cell cultures could impair the epithelial barrier function and secreted various cytokines and chemokines. In order to investigate the potential role of cellular senescence in aged ocular surface, we compared the ocular surfaces in young mice (4 months of age) and old mice (24 months of age). We found that the expression of both p16 and p21 was significantly elevated in the cornea of old mice (**Fig. 4e**). In addition, we detected more punctate epithelial damage in the cornea of old mice compared to young mice (**Fig. 4f,g**), indicating that the epithelial barrier at the ocular surface is disrupted in old mice. We also found that SASP-related genes, including *Il-6*, *Il-1β*, *Mmp3*, and *Tnf-α*, as well as chemokines-related genes, such as *CCL2*, *CXCL3*, *CXCL9*, and *CXCL10*, were elevated in cornea of old mice compared to young mice (**Fig. 4h,i**), suggesting that the SASP secreted by SOC could be responsible for corneal opacity associated with severe angiogenesis in LGE-treated old mice. Interestingly, LGE in young mice did not trigger increased expression of *Cd68* as observed in old mice (**Fig. 4j**), suggesting that the presence of senescent cells is an important factor for the inflammatory phenotypes observed in old mice.

We next examined whether the ocular surface could become opaque at an old age when LGE was performed at a young age (**Fig. 4k**). Eyes that underwent LGE treatment eventually showed corneal opacity, while none of the control eyes (no LGE treatment) displayed corneal opacity during the time frame investigated (**Fig. 4l**). Histological analysis revealed that corneas post LGE displayed a keratinized epithelium associated with an increased number of inflammatory cells (**Fig. 4m**), suggesting that senescent cells exacerbate ocular surface abnormalities during severe DE in aged eyes.

Partial reversibility of angiogenesis upon delayed elimination of p16-positive senescent cells

In order to determine the levels of involvement of senescence cells in corneal opacity during severe DE due to LGE, we attempted to selectively remove senescence cells in old mice using a senolytic approach. We previously reported that our p16-3MR mice allow the selective ablation of p16-positive-senescent cells upon treatment with GCV, a nucleoside analog that has a high affinity for HSV-TK but low affinity for cellular TK, and is converted into a toxic moiety by the HSV-TK[14,37]. Although it is possible to administer GCV systemically, we used topical administration to mimic clinical applications, and determined the therapeutic benefits of eliminating senescent cells upon topical GCV treatment. First, we assessed the effect of 0.3% GCV eye drops for 2 weeks in old mice, and we found that the senescent markers, *p16* and *p21*, as well as the SASP-related genes, *Mmp9* and *Vegf*, were significantly downregulated compared to PBS treatment (**Fig. 5a**).

Next, we examined topical GCV treatment in our experimental DE model. About 0.3% GCV eye drops were administered one month after LGE, three times a day for 5 days for two cycles with a 2-day interval between the cycles (**Fig. 5b**). LGE in old mice drove corneal opacity associated with severe angiogenesis (**Fig. 5c**), and the severity of angiogenesis was partially reduced upon GCV treatment compared to control PBS treatment. Reversal of corneal opacity was also observed upon GCV treatment, whereas PBS-treated eyes worsened as epithelial cell hyperproliferation was observed at the peripheral cornea (**Fig. 5c**). We also determined that gene expression levels of *p16* and some SASP-related genes, *Il-6*, *Il-1β*, *Mmp9*, and *Vegf*, were elevated in control-treated LGE mice, but significantly downregulated upon topical GCV treatment in LGE mice (**Fig. 5d**). Since SOC secrete a variety of chemokines, we examined the expression of *Cd68* and *F4/80* within the ocular surface after LGE. We found these genes elevated in LGE-treated control eyes, but downregulated upon topical GCV treatment (**Fig. 5e**), as what was observed for the expression of SASP-related genes.

Early senolytic treatment protects from corneal opacity in old DE mice

Topical GCV treatment showed partial improvement in eye condition, but the transparency of the cornea was not completely reversed and the corneal opacity remained, which could be due to treatment timing. Therefore, we next tested whether a lower senescence burden triggered by early treatment with topical GCV could prevent corneal opacity and angiogenesis after LGE. Topical GCV treatment was administered starting one week before and finishing one week after LGE (**Fig. 5f**). All LGE-treated eyes became opaque when topical control PBS eye drops were added, while LGE-treated eyes were protected from corneal opacity and angiogenesis when topical GCV eye drops were added (**Fig. 5g**). Finally, two other cases displayed corneal opacity but a reduction in angiogenesis upon treatment with topical GCV. The decrease in senescence burden was associated with a decrease in expression of SASP-related genes and cytokines (**Fig. 5h**). The number of macrophages expressing *Cd68* and *F4/80* was also reduced upon treatment with topical GCV

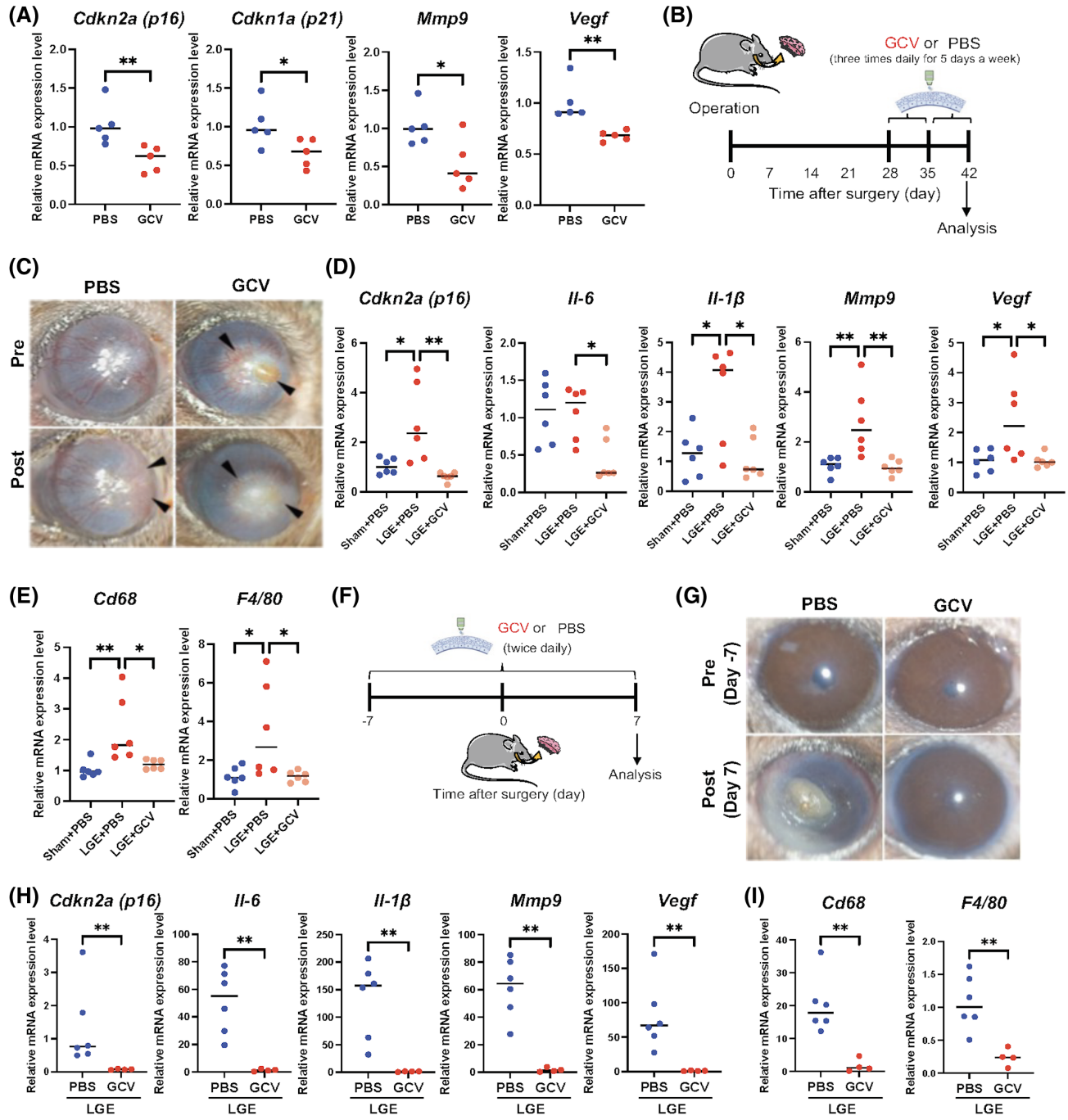

Figure 5. Effects of topical ganciclovir (GCV) at the ocular surface of old p16-3MR mice post LGE. (A) Using real-time PCR, RNA expression analysis of *p16, p21, Mmp9, and Vegf* in the cornea of old p16-3MR mice (24 months of age) treated with GCV (n = 5) or PBS (n = 5) (used as controls). Both topical GCV and PBS were administered three times daily for five days for two cycles with a 2-day interval between the cycles. **(B)** Timeline of treated old p16-3MR mice (24 months of age) after LGE. **(C)** Slit-lamp images of the ocular surface of the cornea of old p16-3MR mice treated with GCV compared to mice treated with PBS (used as controls). Both topical GCV and PBS were administered 3 times daily for 5 days for two cycles with a 2-day interval between the cycles. **(D)** Using real-time PCR, RNA expression analysis of *p16* and SASP factors (*Il-6*, *Il-1β*, *Mmp9*, and *Vegf*) in cornea from old p16-3MR mice after either sham surgery or LGE surgery, and topical PBS (−) or GCV (+) treatment (n = 6 per each group). **(E)** Using real-time PCR, RNA expression analysis of *Cd68* and *F4/80* in cornea from old p16-3MR mice after either sham surgery or LGE surgery, and topical PBS (−) or GCV (+) treatment (n = 6 per each group). **(F)** Timeline of treated old p16-3MR mice (24 months of age) before LGE. **(G)** Slit-lamp images of the ocular surface of the cornea of old p16-3MR mice treated with GCV compared to mice treated with PBS (used as controls). Both topical GCV and PBS were administered 2 times daily for 14 days. **(H)** Using real-time PCR, RNA expression analysis of *p16* and SASP-related genes (*Il-6*, *Il-1β*, *Mmp9*, *Vegf*). **(I)** Using real-time PCR, RNA expression analysis of *Cd68* and *F4/80* in cornea from old p16-3MR mice after LGE surgery, and topical PBS (−) (n = 6) or GCV (+) treatment (n = 4). Gene expression was normalized to the housekeeping gene *Actb*. * = $p < 0.05$; ** = $p < 0.01$. *** = $p < 0.001$.

(Fig. 5i), indicating that elimination of SOC can change the microenvironment at the ocular surface, resulting in protection from corneal opacity and angiogenesis in DE models of aged mice. These findings suggest that reducing the number of SOC at the ocular surface can prevent, or at least reduce, some features of severe DE induced by LGE in old mice.

Discussion

The prevalence of various diseases increases exponentially with aging because of the accumulation of senescent cells[54,55]. So far, there was no report on the ability of ocular surface cells to undergo senescence and on the features of their SASP as a cause of inflammation at the ocular surface. Here, we show that the aging process at the ocular surface is accompanied by an increase in senescence burden and that a senolytic approach protected mice eyes from corneal opacity and angiogenesis in DE models in response to LGE.

One of the biological functions of SOC is the disruption of epithelial barrier function. Studies using human corneas have shown that this function decreases during aging[44,56]. Even though p53 expression has not been described in the cornea, it was reported that the expression of the senescent-associated markers $p16^{INK4a}$ and $p21^{CIP1}$ increased with age in the corneal epithelium of human donors[46]. Similarly, in mouse studies, the barrier function declines, and corneal epithelial damage and corneal permeability increase with age[6,18,49]. We investigated the role of cellular senescence using human cell cultures and *in vivo* mouse models, and we show that the disruption of the epithelial barrier function is a consequence of increased expression $p16^{INK4a}$, $p21^{CIP1}$, and the SASP, ultimately driving impaired ocular surface and signs of DE. We therefore report here an important role for senescent cells at the ocular surface, particularly their ability to alter the microenvironment and their role in the appearance of corneal diseases.

Furthermore, MS analysis of conditioned media from SOC identified an increase of GDF15 and lower levels of LTBP3 in the senescent corneal SASP, which could lead to the activation of TGF-β. TGF-β1 activates NF-κB, resulting in a secondary cellular senescence[46] that exacerbates the inflammatory response. The MMPs identified play an important role in the maintenance of epithelial barrier function, suggesting that they could represent potential biomarkers indicating the decline of ocular surface function during aging. MS analysis also revealed an increase in keratinization and a decrease of neural phenotype. We previously reported that human primary CoC genetically depleted of PAX6, a master regulator of the development and differentiation of eyes and neurons, underwent an upregulation of skin keratinocyte-related genes[24]. Here, we report that SOC gain abnormal behavior compared to NS cells, which could explain the loss of their biological functions.

Another important role of SOC is chronic inflammation due to an SASP generated upon accumulation of senescent cells during aging, which drives several age-related diseases and is linked to many pathological hallmarks of aging[57]. We show that corneas started to become opaque one week after LGE, and when elimination of senescent cells was performed after a month, it still resulted in irreversible scarring of the cornea. However, a treatment using senolytics one week earlier could maintain the cornea transparent even after LGE, suggesting that the prophylactic administration reduces the deleterious effects of senescent cells at the ocular surface, increases the barrier function, and counterbalances the deleterious effects of the ocular SASP, resulting in the maintenance of a healthy ocular surface.

The ocular SASP may explain the link between senescent cells and corneal opacity or angiogenesis. Senescent CoC have been detected at the surface layer of human corneal epithelium[46], and we have also previously reported the presence of p16-positive cells at the surface of human conjunctival epithelium, associated with a decrease in barrier function[58]. Therefore, as shown in old mice, senescent corneal cells could lead to a decline in barrier function and result in epithelial damage. If there is enough tear fluid in old mice, transparency of the cornea is maintained even though corneal epithelial damage occurs due to DE. However, when the lacrimal gland is removed in old mice, SASP proteins in tear fluid, including GDF15, MMP, and vascular endothelial growth factor (VEGF), become concentrated under DE conditions, resulting in stronger ocular phenotypes characterized by corneal opacity and angiogenesis. Similar clinical findings are detected in refractory ocular surface diseases, such as Stevens-Johnson Syndrome[59], graft versus host disease[60], ocular cicatricial pemphigoid[61], or Sjögren's syndrome[62], which are all associated with severe DE.

Therapeutic interventions for DE mainly alleviate the symptoms—for example, by using hyaluronic acid-containing eye drops. Recent studies have shown that regulation of T cell activation using drugs such as cyclosporine or intercellular adhesion molecule-1 inhibitor represents another potential target for DE treatment[63,64]. This is related to the fact that DE can be caused by chronic inflammation. However, it is still unclear how chronic inflammation exerts its effects during DE, and the links between SOCs and inflammation in the eye still need to be investigated.

The SASP can act in a paracrine manner to alter the organization and function of neighboring normal cells. Even though secondary senescence was not investigated in our study, we determined that cellular senescence at the ocular surface participated in the pathophysiology of DE and that elimination of senescent cells protected from corneal opacity. The extensive characterization of the ocular SASP could lead to the development of diagnostic tools and treatments based on the presence of SOC and on the use of senolytic agents.

Acknowledgments

The authors thank Masahiro Nakamura, Pacome Lecot, Jun-Wei B. Hughes, Chisaka Kuehnemann, Francesco Neri, and Corey Webster for helpful scientific discussion. The work was supported by the National Institutes of Health grants R01 AG009909 and P01 AG017242 (J.C.), and U01 AG060906 (B.S.), and partly supported by a Glenn Foundation fellowship (S.K.P.), and by the Japan Society for the Promotion of Science (#201960725), Japan Eye Bank Association, and Alcon Novartis Hida Memorial Award 2017 (K.K.).

Author Contributions

K.K., P.-Y.D., B.S., and J.C. designed the experiments; K.K., K.N., S.K.P., C.D.K., and A.M. conducted the experiments; K.K., P.Y.D., B.S., and J.C. analyzed the data; K.K., S.K.P., A.M., C.S., P.Y.D., B.S., and J.C. wrote or edited this article.

Competing Financial Interests

The authors declare no competing financial interests. J.C. is a founder of Unity Biotechnology, which develops methods to eliminate senescent cells.

Data Availability Statement

Raw data and complete Mass Spectrometry (MS) datasets have been uploaded to the Mass Spectrometry Interactive Virtual Environment (MassIVE) repository, developed by the Center for Computational Mass Spectrometry at the University of California, San Diego, and can be downloaded using the following link: ftp://MSV000090204@massive.ucsd.edu (MassIVE ID number: MSV000090204; ProteomeXchange ID: PXD036253). Raw dataset for RNA-seq was deposited in Gene Expression Omnibus (GEO) (accession number: GSE232508).

Supplementary Materials

Supplemental information can be found online at https://doi.org/10.59368/agingbio.20230014.

Accepted August 7, 2023
Published September 15, 2023

References

1. Kitazawa K., Inomata T., Shih K., Hughes J.B., Bozza N., Tomioka Y., … Sotozono C. (2022). Impact of aging on the pathophysiology of dry eye disease: A systematic review and meta-analysis. *Ocul. Surf.* **25**, 108–118. PMID: 35753664; doi: 10.1016/j.jtos.2022.06.004.
2. Giebel J., Woenckhaus C., Fabian M., & Tost F. (2005). Age-related differential expression of apoptosis-related genes in conjunctival epithelial cells. *Acta. Ophthalmol. Scand.* **83**(4), 471–476. PMID: 16029273; doi: 10.1111/j.1600-0420.2005.00472.x.
3. Nien C.J., Massei S., Lin G., Nabavi C., Tao J., Brown D.J., … Jester J.V. (2011). Effects of age and dysfunction on human meibomian glands. *Arch. Ophthalmol.* **129**(4), 462–469. PMC4291168. PMID: 21482872; doi: 10.1001/archophthalmol.2011.69.
4. Parfitt G.J., Xie Y., Geyfman M., Brown D.J., & Jester J.V. (2013). Absence of ductal hyper-keratinization in mouse age-related meibomian gland dysfunction (ARMGD). *Aging (Albany NY)* **5**(11), 825–834. PMC3868725. PMID: 24259272; doi: 10.18632/aging.100615.
5. Parfitt G.J., Brown D.J., & Jester J.V. (2016). Transcriptome analysis of aging mouse meibomian glands. *Mol. Vis.* **22**, 518–527. PMC4880544. PMID: 27279727.
6. Yoon C.H., Ryu J.S., Hwang H.S., & Kim M.K. (2020). Comparative analysis of age-related changes in lacrimal glands and meibomian glands of a C57BL/6 male mouse model. *Int. J. Mol. Sci.* **21**(11), 4169. PMC7313015. PMID: 32545199; doi: 10.3390/ijms21114169.
7. Lopez-Otin C., Blasco M.A., Partridge L., Serrano M., & Kroemer G. (2013). The hallmarks of aging. *Cell* **153**(6), 1194–1217. PMC3836174. PMID: 23746838; doi: 10.1016/j.cell.2013.05.039.
8. Furman D., Campisi J., Verdin E., Carrera-Bastos P., Targ S., Franceschi C., … Slavich G.M. (2019). Chronic inflammation in the etiology of disease across the life span. *Nat. Med.* **25**(12), 1822–1832. PMC7147972. PMID: 31806905; doi: 10.1038/s41591-019-0675-0.
9. Herranz N., & Gil J. (2018). Mechanisms and functions of cellular senescence. *J. Clin. Invest.* **128**(4), 1238–1246. PMC5873888. PMID: 29608137; doi: 10.1172/JCI95148.
10. Hayflick L., & Moorhead P.S. (1961). The serial cultivation of human diploid cell strains. *Exp. Cell Res.* **25**, 585–621. PMID: 13905658; doi: 10.1016/0014-4827(61)90192-6.
11. Campisi J. (2005). Senescent cells, tumor suppression, and organismal aging: Good citizens, bad neighbors. *Cell* **120**(4), 513–522. PMID: 15734683; doi: 10.1016/j.cell.2005.02.003.
12. Coppe J.P., Patil C.K., Rodier F., Sun Y., Munoz D.P., Goldstein J., … Campisi J. (2008). Senescence-associated secretory phenotypes reveal cell-nonautonomous functions of oncogenic RAS and the p53 tumor suppressor. *PLoS Biol.* **6**(12), 2853–2868. 2592359. PMID: 19053174; doi: 10.1371/journal.pbio.0060301.
13. Basisty N., Kale A., Jeon O.H., Kuehnemann C., Payne T., Rao C., … Schilling B. (2020). A proteomic atlas of senescence-associated secretomes for aging biomarker development. *PLoS Biol.* **18**(1), e3000599. PMC6964821 following competing interests: JC is a founder and shareholder of Unity Biotechnology, which develops senolytic drugs. All other authors have declared no competing interests. PMID: 31945054; doi: 10.1371/journal.pbio.3000599.
14. Jeon O.H., Kim C., Laberge R.M., Demaria M., Rathod S., Vasserot A.P., … Elisseeff J.H. (2017). Local clearance of senescent cells attenuates the development of post-traumatic osteoarthritis and creates a pro-regenerative environment. *Nat. Med.* **23**(6), 775–781. 5785239. PMID: 28436958; doi: 10.1038/nm.4324.
15. Chang J., Wang Y., Shao L., Laberge R.M., Demaria M., Campisi J., … Zhou D. (2016). Clearance of senescent cells by ABT263 rejuvenates aged hematopoietic stem cells in mice. *Nat. Med.* **22**(1), 78–83. PMC4762215. PMID: 26657143; doi: 10.1038/nm.4010.
16. Childs B.G., Baker D.J., Wijshake T., Conover C.A., Campisi J., & van Deursen J.M. (2016). Senescent intimal foam cells are deleterious at all stages of atherosclerosis. *Science* **354**(6311), 472–477. PMC5112585. PMID: 27789842; doi: 10.1126/science.aaf6659.
17. De Paiva C.S., Villarreal A.L., Corrales R.M., Rahman H.T., Chang V.Y., Farley W.J., … Pflugfelder S.C. (2007). Dry eye-induced conjunctival epithelial squamous metaplasia is modulated by interferon-gamma. *Invest. Ophthalmol. Vis. Sci.* **48**(6), 2553–2560. PMID: 17525184; doi: 10.1167/iovs.07-0069.
18. Bian F., Xiao Y., Barbosa F.L., de Souza R.G., Hernandez H., Yu Z., … de Paiva C.S. (2019). Age-associated antigen-presenting cell alterations promote dry-eye inducing Th1 cells. *Mucosal. Immunol.* **12**(4), 897–908. PMC6599474. PMID: 30696983; doi: 10.1038/s41385-018-0127-z.
19. Kitazawa K., Hikichi T., Nakamura T., Mitsunaga K., Tanaka A., Nakamura M., … Masui S. (2016). OVOL2 maintains the transcriptional program of human corneal epithelium by suppressing epithelial-to-mesenchymal transition. *Cell Rep.* **15**(6), 1359–1368. PMID: 27134177; doi: 10.1016/j.celrep.2016.04.020.
20. Nakamura T., Yokoo S., Bentley A.J., Nagata M., Fullwood N.J., Inatomi T., … Kinoshita S. (2016). Development of functional human oral mucosal epithelial stem/progenitor cell sheets using a feeder-free and serum-free culture system for ocular surface reconstruction. *Sci. Rep.* **6**, 37173. 5107917. PMID: 27841343; doi: 10.1038/srep37173.
21. Demaria M., O'Leary M.N., Chang J., Shao L., Liu S., Alimirah F., … Campisi J. (2017). Cellular senescence promotes adverse effects of chemotherapy and cancer relapse. *Cancer Discov.* **7**(2), 165–176. PMC5296251. PMID: 27979832; doi: 10.1158/2159-8290.CD-16-0241.
22. Chang B.D., Swift M.E., Shen M., Fang J., Broude E.V., & Roninson I.B. (2002). Molecular determinants of terminal growth arrest induced in tumor cells by a chemotherapeutic agent. *Proc. Natl. Acad. Sci. U. S. A.* **99**(1), 389–394. PMC117570. PMID: 11752408; doi: 10.1073/pnas.012602599.
23. Alimirah F., Pulido T., Valdovinos A., Alptekin S., Chang E., Jones E., … Campisi J. (2020). Cellular senescence promotes skin carcinogenesis through p38MAPK and p44/42MAPK signaling. *Cancer Res.* **80**(17), 3606–3619. PMC7484313. PMID: 32641409; doi: 10.1158/0008-5472.CAN-20-0108.
24. Kitazawa K., Hikichi T., Nakamura T., Sotozono C., Kinoshita S., & Masui S. (2017). PAX6 regulates human corneal epithelium cell identity. *Exp. Eye Res.* **154**, 30–38. PMID: 27818314; doi: 10.1016/j.exer.2016.11.005.
25. Kitazawa K., Kawasaki S., Shinomiya K., Aoi K., Matsuda A., Funaki T., … Kinoshita S. (2013). Establishment of a human corneal epithelial cell line lacking the functional TACSTD2 gene as an in vitro model for gelatinous drop-like dystrophy. *Invest. Ophthalmol. Vis. Sci.* **54**(8), 5701–5711. PMID: 23868985; doi: 10.1167/iovs.12-11043.
26. Andrews S. (2010). FastQC: A quality control tool for high throughput sequence data. Accessed on 31 July 2023. http://www.bioinformatics.babraham.ac.uk/projects/fastqc/.

27. Martin M.P. (2011). Cutadapt removes adapter sequences from high-throughput sequencing reads. *EMBnet Journal* **17**, 10–12. PMID: 28715235; doi: 10.1089/cmb.2017.0096.

28. Kim D., Langmead B., & Salzberg S.L. (2015). HISAT: A fast spliced aligner with low memory requirements. *Nat. Methods* **12**(4), 357–360. PMC4655817. PMID: 25751142; doi: 10.1038/nmeth.3317.

29. Li H. Handsaker B., Wysoker A., Fennell T., Ruan J., Homer N. , … Genome Project Data Processing S (2009). The sequence alignment/map format and SAMtools. *Bioinformatics* **25**(16), 2078–2079. 2723002. PMID: 19505943; doi: 10.1093/bioinformatics/btp352.

30. Liao Y., Smyth G.K., & Shi W. (2014). featureCounts: An efficient general purpose program for assigning sequence reads to genomic features. *Bioinformatics* **30**(7), 923–930. PMID: 24227677; doi: 10.1093/bioinformatics/btt656.

31. Love M.I., Huber W., & Anders S. (2014). Moderated estimation of fold change and dispersion for RNA-seq data with DESeq2. *Genome. Biol.* **15** (12), 550. PMC4302049. PMID: 25516281; doi: 10.1186/s13059-014-0550-8.

32. Escher C., Reiter L., MacLean B., Ossola R., Herzog F., Chilton J., … Rinner O. (2012). Using iRT, a normalized retention time for more targeted measurement of peptides. *Proteomics* **12**(8), 1111–1121. PMC3918884. PMID: 22577012; doi: 10.1002/pmic.201100463.

33. Gillet L.C., Navarro P., Tate S., Rost H., Selevsek N., Reiter L., … Aebersold R. (2012). Targeted data extraction of the MS/MS spectra generated by data-independent acquisition: A new concept for consistent and accurate proteome analysis. *Mol. Cell Proteomics* **11**(6), O111 016717. PMC3433915. PMID: 22261725; doi: 10.1074/mcp.O111.016717.

34. Bruderer R., Bernhardt O.M., Gandhi T., Xuan Y., Sondermann J., Schmidt M., … Reiter L. (2017). Optimization of experimental parameters in data-independent mass spectrometry significantly increases depth and reproducibility of results. *Mol. Cell Proteomics* **16**(12), 2296–2309. PMC5724188. PMID: 29070702; doi: 10.1074/mcp.RA117.000314.

35. Collins B.C., Hunter C.L., Liu Y., Schilling B., Rosenberger G., Bader S.L., … Aebersold R. (2017). Multi-laboratory assessment of reproducibility, qualitative and quantitative performance of SWATH-mass spectrometry. *Nat. Commun.* **8**(1), 291. PMC5566333. PMID: 28827567; doi: 10.1038/s41467-017-00249-5.

36. Burger T. (2018). Gentle introduction to the statistical foundations of false discovery rate in quantitative proteomics. *J. Proteome. Res.* **17**(1), 12–22. PMID: 29067805; doi: 10.1021/acs.jproteome.7b00170.

37. Demaria M., Ohtani N., Youssef S.A., Rodier F., Toussaint W., Mitchell J.R., … Campisi J. (2014). An essential role for senescent cells in optimal wound healing through secretion of PDGF-AA. *Dev. Cell.* **31**(6), 722–733. PMC4349629. PMID: 25499914; doi: 10.1016/j.devcel.2014.11.012.

38. Baker D.J., Wijshake T., Tchkonia T., LeBrasseur N.K., Childs B.G., van de Sluis B., … van Deursen J.M. (2011). Clearance of p16Ink4a-positive senescent cells delays ageing-associated disorders. *Nature* **479** (7372), 232–236. PMC3468323. PMID: 22048312; doi: 10.1038/nature10600.

39. Baker D.J., Childs B.G., Durik M., Wijers M.E., Sieben C.J., Zhong J., … van Deursen J.M. (2016). Naturally occurring p16(Ink4a)-positive cells shorten healthy lifespan. *Nature* **530**(7589), 184–189. PMC4845101. PMID: 26840489; doi: 10.1038/nature16932.

40. Shinomiya K., Ueta M., & Kinoshita S. (2018). A new dry eye mouse model produced by exorbital and intraorbital lacrimal gland excision. *Sci. Rep.* **8** (1), 1483. PMC5784089. PMID: 29367638; doi: 10.1038/s41598-018-19578-6.

41. Coppe J.P., Desprez P.Y., Krtolica A., & Campisi J. (2010). The senescence-associated secretory phenotype: The dark side of tumor suppression. *Annu. Rev. Pathol.* **5**, 99–118. PMC4166495. PMID: 20078217; doi: 10.1146/annurev-pathol-121808-102144.

42. Freund A., Laberge R.M., Demaria M., & Campisi J. (2012). Lamin B1 loss is a senescence-associated biomarker. *Mol. Biol. Cell.* **23**(11), 2066–2075. PMC3364172. PMID: 22496421; doi: 10.1091/mbc.E11-10-0884.

43. Parrinello S., Coppe J.P., Krtolica A., & Campisi J. (2005). Stromal-epithelial interactions in aging and cancer: Senescent fibroblasts alter epithelial cell differentiation. *J. Cell. Sci.* **118**(Pt 3), 485–496. PMC4939801. PMID: 15657080; doi: 10.1242/jcs.01635.

44. Chang S.W., & Hu F.R. (1993). Changes in corneal autofluorescence and corneal epithelial barrier function with aging. *Cornea* **12**(6), 493–499. PMID: 8261780; doi: 10.1097/00003226-199311000-00006.

45. Campisi J., & d'Adda di Fagagna F. (2007). Cellular senescence: When bad things happen to good cells. *Nat. Rev. Mol. Cell. Biol.* **8**(9), 729–740. PMID: 17667954; doi: 10.1038/nrm2233.

46. Li Z.Y., Chen Z.L., Zhang T., Wei C., & Shi W.Y. (2016). TGF-beta and NF-kappaB signaling pathway crosstalk potentiates corneal epithelial senescence through an RNA stress response. *Aging (Albany NY)* **8**(10), 2337–2354. PMC5115892. PMID: 27713146; doi: 10.18632/aging.101050.

47. Martin N., & Bernard D. (2018). Calcium signaling and cellular senescence. *Cell Calcium* **70**, 16–23. PMID: 28410770; doi: 10.1016/j.ceca.2017.04.001.

48. Shikama Y., Kurosawa M., Furukawa M., Ishimaru N., & Matsushita K. (2019). Involvement of adiponectin in age-related increases in tear production in mice. *Aging (Albany NY)* **11**(19), 8329–8346. PMC6814586. PMID: 31596727; doi: 10.18632/aging.102322.

49. McClellan A.J., Volpe E.A., Zhang X., Darlington G.J., Li D.Q., Pflugfelder S.C., & de Paiva C.S. (2014). Ocular surface disease and dacryoadenitis in aging C57BL/6 mice. *Am. J. Pathol.* **184**(3), 631–643. PMC3936306. PMID: 24389165; doi: 10.1016/j.ajpath.2013.11.019.

50. Stevenson W., Chen Y., Lee S.M., Lee H.S., Hua J., Dohlman T., … Dana R. (2014). Extraorbital lacrimal gland excision: A reproducible model of severe aqueous tear-deficient dry eye disease. *Cornea* **33**(12), 1336–1341. PMID: 25255136; doi: 10.1097/ICO.0000000000000264.

51. Guzman M., Keitelman I., Sabbione F., Trevani A.S., Giordano M.N., & Galletti J.G. (2016). Mucosal tolerance disruption favors disease progression in an extraorbital lacrimal gland excision model of murine dry eye. *Exp. Eye Res.* **151**, 19–22. PMID: 27443502; doi: 10.1016/j.exer.2016.07.004.

52. Kim C.S., Jo K., Lee I.S., & Kim J. (2016). Topical application of apricot kernel extract improves dry eye symptoms in a unilateral exorbital lacrimal gland excision mouse. *Nutrients* **8**(11), PMC5133132. PMID: 27886047; doi: 10.3390/nu8110750.

53. Mecum N.E., Cyr D., Malon J., Demers D., Cao L., & Meng I.D. (2019). Evaluation of corneal damage after lacrimal gland excision in male and female mice. *Invest. Ophthalmol. Vis. Sci.* **60**(10), 3264–3274. PMC6675517. PMID: 31369671; doi: 10.1167/iovs.18-26457.

54. Ovadya Y., Landsberger T., Leins H., Vadai E., Gal H., Biran A., … Krizhanovsky V. (2018). Impaired immune surveillance accelerates accumulation of senescent cells and aging. *Nat. Commun.* **9**(1), 5435. PMC6303397. PMID: 30575733; doi: 10.1038/s41467-018-07825-3.

55. Ressler S., Bartkova J., Niederegger H., Bartek J., Scharffetter-Kochanek K., Jansen-Durr P., & Wlaschek M. (2006). p16INK4A is a robust in vivo biomarker of cellular aging in human skin. *Aging Cell* **5**(5), 379–389. PMID: 16911562; doi: 10.1111/j.1474-9726.2006.00231.x.

56. Azcarate P.M., Venincasa V.D., Feuer W., Stanczyk F., Schally A.V., & Galor A. (2014). Androgen deficiency and dry eye syndrome in the aging male. *Invest. Ophthalmol. Vis. Sci.* **55**(8), 5046–5053. PMC4132553. PMID: 24994872; doi: 10.1167/iovs.14-14689.

57. Campisi J., & Robert L. (2014). Cell senescence: Role in aging and age-related diseases. *Interdiscip. Top Gerontol.* **39**, 45–61. PMC4211612. PMID: 24862014; doi: 10.1159/000358899.

58. Tomioka Y., Kitazawa K., Numa K., Yokoi N., & Sotozono C. (2023). UVA-induced cellular senescence in human conjunctival epithelium. *Invest. Ophthalmol. Vis. Sci.* **64**(8), 2028.

59. Sotozono C., Ueta M., & Kinoshita S. (2021). Japan: Diagnosis and management of Stevens-Johnson Syndrome/Toxic Epidermal Necrolysis with severe ocular complications. *Front Med. (Lausanne)* **8**, 657327. PMC8355416. PMID: 34395463; doi: 10.3389/fmed.2021.657327.

60. Wolff D., Radojcic V., Lafyatis R., Cinar R., Rosenstein R.K., Cowen E.W., … Paczesny S. (2021). National Institutes of Health Consensus Development

Project on Criteria for Clinical Trials in Chronic Graft-versus-Host Disease: IV. The 2020 highly morbid forms report. *Transplant Cell Ther.* **27** (10), 817–835. PMC8478861. PMID: 34217703; doi: 10.1016/j.jtct.2021.06.001.

61. Branisteanu D.C., Stoleriu G., Branisteanu D.E., Boda D., Branisteanu C.I., Maranduca M.A., … Balta F. (2020). Ocular cicatricial pemphigoid (review). *Exp. Ther. Med.* **20**(4), 3379–3382. PMC7465597. PMID: 32905166; doi: 10.3892/etm.2020.8972.
62. Donthineni P.R., Doctor M.B., Shanbhag S., Kate A., Galor A., Djalilian A.R., … Basu S. (2023). Aqueous-deficient dry eye disease: Preferred practice pattern guidelines on clinical approach, diagnosis, and management. *Indian J. Ophthalmol.* **71**(4), 1332–1347. PMC10276701. PMID: 37026265; doi: 10.4103/IJO.IJO_2808_22.
63. Keating G.M. (2017). Lifitegrast ophthalmic solution 5%: A review in dry eye disease. *Drugs* **77**(2), 201–208. PMID: 28058622; doi: 10.1007/s40265-016-0681-1.
64. Baiza-Duran L., Medrano-Palafox J., Hernandez-Quintela E., Lozano-Alcazar J., & Alaniz-de la O.J. (2010). A comparative clinical trial of the efficacy of two different aqueous solutions of cyclosporine for the treatment of moderate-to-severe dry eye syndrome. *Br. J. Ophthalmol.* **94**(10), 1312–1315. PMID: 20679084; doi: 10.1136/bjo.2008.150011.